Chapter 5

Electron spectroscopy

5.1 Electron interactions

Effects upon bombardment of material with electron beam:

- material processing: cleaning (desorption), activation energy for chemical and physical processes, electron lithography
- heating: evaporation
- reflection, transmission
- diffraction (scattering)
- excitation of photons (x-ray, chatodoluminescence)
- emission of true secondary electrons

Total electron current from a substance is the current of *secondary electrons* on reflection or transmission. Different processes that lead to this current are depicted in Fig. 5.1. The *true secondary electrons* are part of it. The secondary electron yield depends on many factors, and is generally higher for high atomic number targets, and at higher angles of incidence. In Fig. 5.2, there is a general division of different characterization methods that uses emitted electrons.

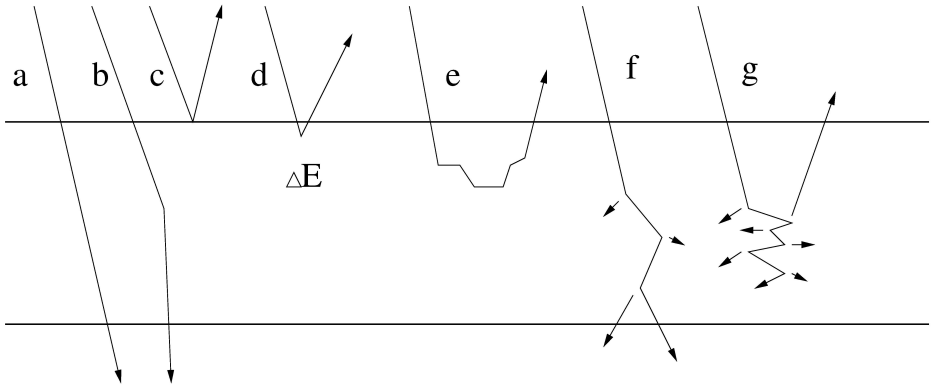

Figure 5.1: Electron emission: (a) without interaction, (b) elastic scattering (diffraction on passage), (c) elastic reflection (diffraction on reflection), (d) inelastic reflection (characteristic energy loss), (e) backscatter electron, (f) electron transmission with the possibility to emit others and (g) electron transmission with secondary electron emission.

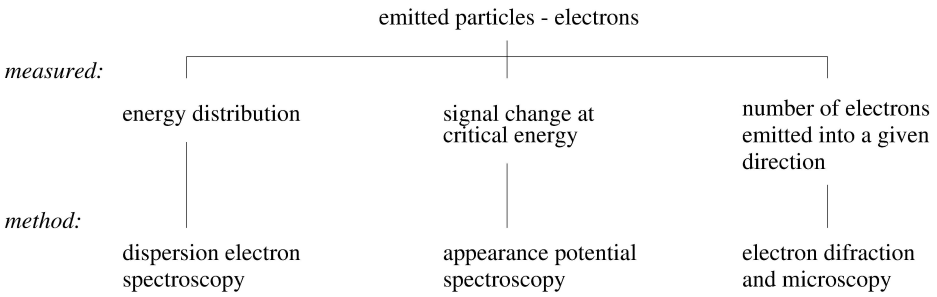

Figure 5.2: Overwiev of measuring methods that use emitted electrons.

The ration between this current I_s and primary I_p is called **secondary emission coefficient** $\sigma = I_s/I_p$. Looking at the energy distribution of the secondary electrons (Fig. 5.3) we can identify individual interactions:

- the highest maximum of primary energy level ⇒ elastic reflection of e^-
  interaction with the atom like a whole, there is no change in energy but, the electron momentum can be changed dramatically. For higher energies (≥ 5 keV), it can be described by Rutherford scattering

$$\frac{dQ(\theta)}{d\Omega} = \frac{1}{4}\left(\frac{e^2\ (Z - F(\theta))}{4\pi\epsilon_0\ m_{\text{red}}\ g^2}\right)^2 \frac{1}{\sin^4(\theta/2)}, \tag{5.1}$$

  where $F(\theta)$ is the screening effect of electrons. $F(\theta)$ is insignificant at high angles θ and strong scattering can occur only in heavy atoms (used for TEM contrast). When the target is a crystalline material **diffraction** and **channelling** occurs. When electron scattering from crystal lattice is coherent, amplification in those direction occurs, which is represents **Bragg law**:

$$n\lambda = 2d_{\text{hkl}} \sin\theta, \tag{5.2}$$

  where n is a integer d_{hkl} is is the spacing between the planes in the atomic lattice expressed with Miller indexes. This method is used to examine the bulk crystalline structure ($E \approx$ 10 keV) or the surface structure using low-energy electron diffraction (LEED) or very small angle relection in reflection high-energy electron diffraction (RHEED).

- smaller peaks on the left exhibit energy shift together with the maximum of elastic scattered electrons ⇒ electrons which suffered some characteristic energy loss:

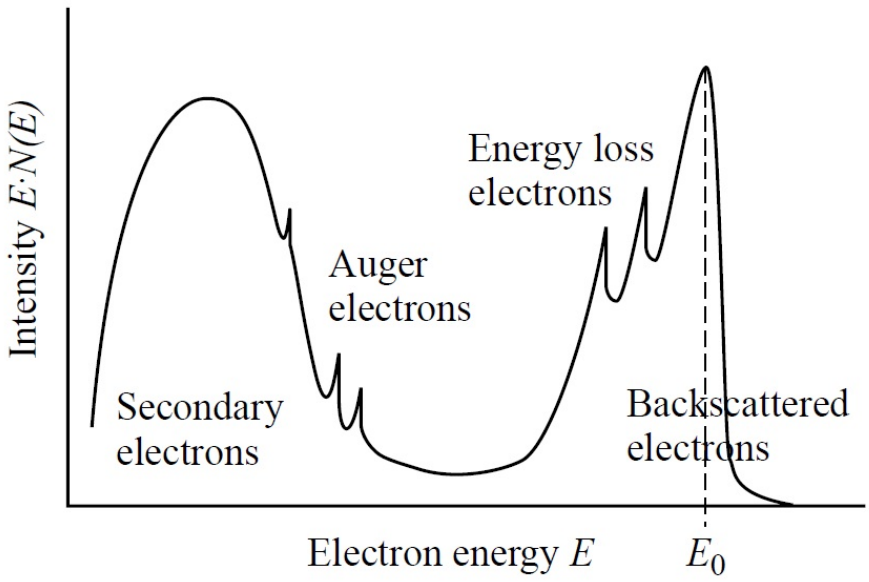

Figure 5.3: Electron energy distribution.

- excitation of vibrational states in adsorbed molecules $\Delta E \approx 50$–500 meV;
- individual interaction with valence e^-, $\Delta E \approx 3$–20 eV but this interaction does not have a sharp value because the valence band has a width of several eV
- interaction with the cloud of e^-having characteristic oscillation frequency - excitation of plasmon with the frequency of

$$\omega_\mathrm{p} = \sqrt{\frac{1}{\epsilon_0}\,\frac{n_0 e^2}{m}} \tag{5.3}$$

for plasmon in volume, or

$$\omega_\mathrm{s} = \frac{\omega_\mathrm{p}}{\sqrt{1+\epsilon_r}} = \frac{\omega}{\sqrt{2}} \tag{5.4}$$

for excitation of the surface plasmon. ΔE is between 5 and 60 eV.

- broader peak at low energies - true secondary electrons, usually defined with the condition $E < 45 - 50$ eV
- Usually, electrons undergo many inelastic interactions (phonon excitations, inter and intra band transitions, plasmon excitations, inner shell ionizations) and when emitted as "back diffusion" they do not bring a specific information (background signal that also includes a small part of fast true secondary electrons). Small part of electrons are emitted after undergoing only one such interaction - only electrons emitted from a thin surface layer or through a thin specimen $\Rightarrow$ **electron energy loss spectroscopy** (EELS).
- smaller peaks on the signal of true secondary electrons (left part of the EEDF) - do not shift with energy of primary beam $\Rightarrow$ **Auger** e^- which have for each substance a characteristic position.

  The process is following. Primary e^- removes a core e^- (e.g. from K shell) creating a hole. As this is an unstable state, the core hole can be filled by an outer shell electron, whereby the electron moving to the lower energy level loses an amount of energy equal to the difference in orbital energies. The transition energy can be coupled to a second outer shell electron which will be emitted from the atom if the transferred energy is greater than the orbital binding energy. The Auger energy released

$$E_\mathrm{k} = E_\mathrm{K} - E_\mathrm{L} - E'_\mathrm{V} - E_\mathrm{af}. \tag{5.5}$$

  The E'_V is not equal with the original level energy E_V, because the e^- on the level V moves in a potential and the e^- on the level L is missing. The Auger requires the existence of at least two energy levels to three electrons. That is why it can not measure H and He. The elements with atomic number between 3 and 14 have KLL line, elements between 14 and 40 have LMM line, between 40 and 79 are MNN line and for heavier elements NOO line exists.

5.2 Spectroscopic methods involving electrons

Dispersive electron spectroscopies:

- UPS - Ultraviolet Photoelectron Spectroscopy using VUV radiation, especially from synchrotron; excitation of electrons from valence band;
- XPS - X-ray Photoelectron Spectroscopy (ESCA - Electron Spectroscopy for Chemical Analysis) using soft X-rays; excitation of electrons from core levels;
- AES - Auger Electron Spectroscopy (remember Auger electron effect discussed before);
- EELS - Electron Energy Loss Spectroscopy, used in the case of internal excitation of electron levels (inter and intraband transitions, plasmons, excitation of phonons) or IS - Ionization Spectroscopy (energy losses due to the excitation of core electrons);
- INS - Ion Neutralization Spectroscopy (slow ions neutralize after impingment and transmit part of the energy to electrons that are emitted)
- FES - Field Electron Spectroscopy, energy distribution measurements of field-emitted electrons

Notice: The method called XAS (X-ray absorption spectroscopy) does not belong to electron spectroscopies but uses the principles of UPS and XPS - absorption of photons due to excitation of electrons.

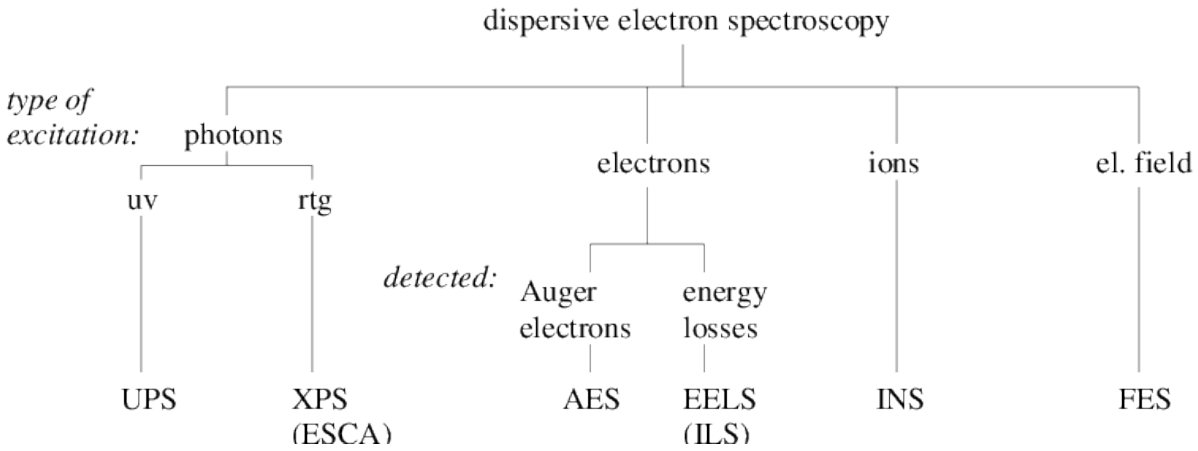

Figure 5.4: Overwiev of different dispersive electron spectroscopy methods. UPS - Ultraviolet Photoelectron Spectroscopy, XPS - X-ray Photoelectron Spectroscopy, AES - Auger Electron Spectroscopy, EEELS - Electron Energy Loss Spectroscopy, used in the case of internal excitation of electron levels, also known as IS - Ionization Spectroscopy, INS - Ion Neutralization Spectroscopy, FES - Field Electron Spectroscopy, energy distribution measurements of field-emitted electrons

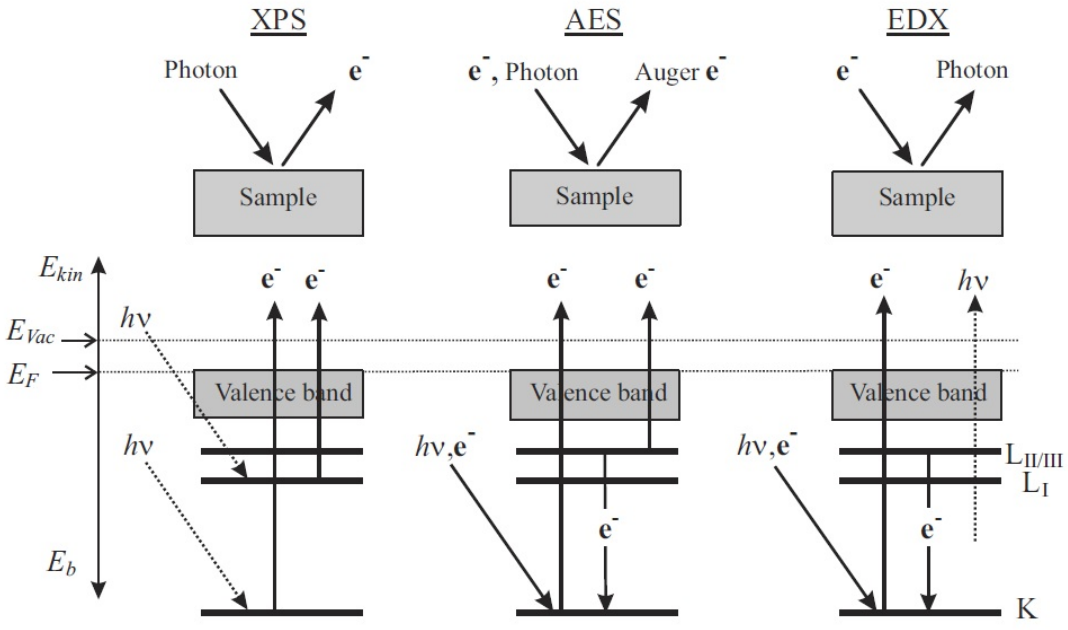

Figure 5.5: Schematic drawing of method's differences.

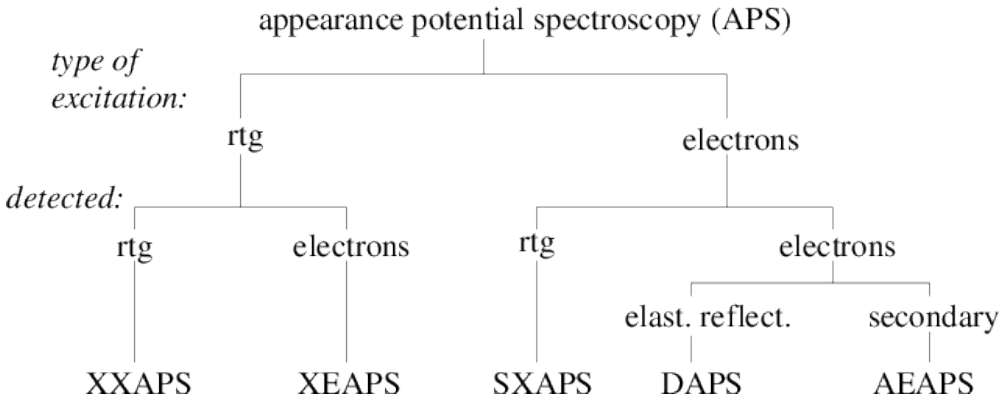

Figure 5.6: Overwiev of different APS methods

Appearance potential spectroscopies:

- XXAPS, XEAPS - X-ray X-ray Appearance Potential Spectroscopy, X-ray Electron Appearance Potential Spectroscopy. Methods in which X-rays are generated from the sample. They are practically not used since electron generation is much easier.
- SXAPS - Soft X-ray APS, electrons impact the sample and emitted X-rays are detected.
- DAPS - Disappearance Potential Spectroscopy, used to measure the surface electrons current.
- AEAPS - Auger Electron APS, records the secondary electrons current.

5.3 Electron spectroscopy conditions

All methods except FES require a **monochromatic source** - more or less focused, a **analyser** and a **detector** (electron multiplier). All this system must be kept under high vacuum conditions ($\leq 10^{-7}$ Pa). If the surface sensitivity is greater, i.e. information depth is smaller, the vacuum conditions must be stronger. The most stringent conditions for surface are for UPS and not so for XPS. The device is equipped with a surface cleaning systems (Ar^+ sputtering and baking) or for preparation of clean surfaces in situ (cleaving or applying of layers).

5.3.1 Sources of primary particles

X-rays: soft X-rays are generated by bombardment of a suitable material (Al, Mg, Mo, Co, W) with sufficient e^- energy $\Rightarrow$ characteristic X-rays.

- Line width limits the resolution ($E_k = h\nu - E_B - e\phi$). Natural line width provides the resolution of ≈ 1.0 eV, monochromatized sources provide better resolution.
- The energy must be high enough in order to obtain emission of photoelectrons from the bulk of material.

- In addition, the anode material needs to be capable of manufacturing into the shape of anode and stable under e^-bombardment.

$\Rightarrow$ Mg Kα ($E = 1253.6$ eV, $\delta E = 0.7$ eV), Al Kα ($E = 1486.6$ eV, $\delta E = 0.85$ eV).
Photoemission starts at e^-energies equal with electron ionization threshold for the inner shell and growing rapidly with increasing energy. Therefore, devices allow e^- acceleration up to 15 keV.

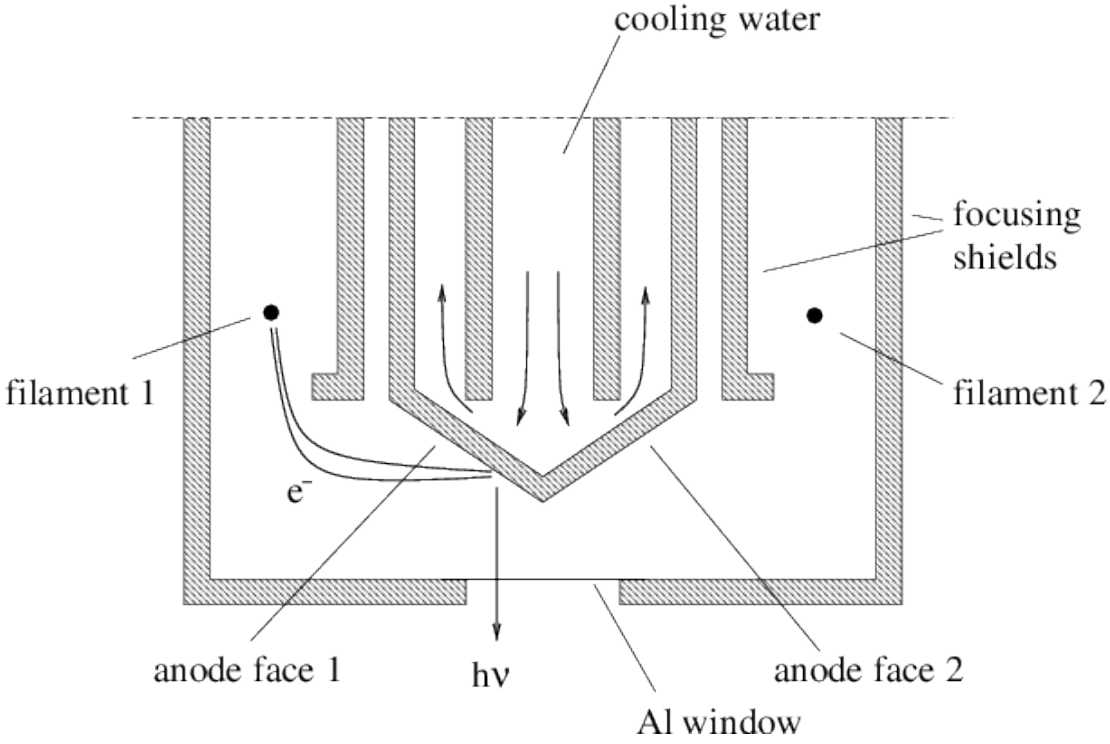

Figure 5.7: Scheme of X - ray source.

The e^- source as close as possible to the anode. The X-ray source is often composed of two anodes. For continuous operation at 1–8 kW, a rotating anode is required. Beside the characteristic lines (Kα for Mg and Al), satellite, Kβ and continuous spectrum (Bremsstrahlung) lines exists. Monochromatic radiation is used to get rid of other signals and also to improve the resolution: Bragg diffraction from a crystal - suitable material is quartz (suitable distance of crystal planes, possible to bend into a shape of Rowland focusing sphere with the radius of 0.5 m).

Synchrotron radiation
If the charged particles are accelerated, they radiate energy which covers an area of electromagnetic radiation from hard X-rays up to IR. The synchrotron is a particular type of cyclic particle accelerator in which the magnetic field (to turn the particles so they circulate) and the electric field (to accelerate the particles) are carefully synchronised with the travelling particle beam. Synchrotron radiation has many advantages: a broad spectrum, natural collimation, high intensity, coherence, the source is under vacuum. Maximum intensity is at the critical wavelength (0.1–0.4 nm) that is related to curvature of e^-path. The intensity decreases rapidly for lower

wavelengths.

Sources of electrons thermionic or field-emission guns. AES does not need a monochromatic e^- source, only electrons with the sufficient energy to ionize the core levels. Energy width of the beam is important for EELS, max. 0.3–0.5 eV, which is too large for HREELS equiring special monochromatic electron sources.

5.3.2 Electron energy analysers

The electron spectroscopy uses electrostatic analysers. The measured values can be divided into

- retarding field analyzers - recording the total current of particles,
- dispersive analyzers - selecting only certain e^-energies by changing the trajectories.

When choosing the analyser following parameters are considered:

- resolution $R = E/\Delta E$ - indicates the spectrum energy resolution;
- intensity (brightness) - affects the intensity of the output signal (signal-to-noise ratio);
- analyzer size - because it needs to be placed in the vacuum chamber;
- complexity - economic factor

The final solution is a compromise because the individual requirements have a contradictory character.

Analysers with retarding field

The operation principle is based on the application of a potential barrier V_b. The flux of particles over the barrier is divided into fast and slow components. Only the faster ones are usually recorded:

$$J(E) = \int_E^\infty N(E')dE', \tag{5.6}$$

where $N(E')$ is the energy distribution of particles, $E = eV_\mathrm{b}$ is the lower energy limit and the symbol ∞ upper limit (maximum energy of particles). The energy distribution function can be obtained from the derivative of the above equation.

Planar analyser

The analyzed beam is usually selected by an entrance slit which properties are crucial for the accuracy of the energy measurements. Since it divides the space without and with the decelating field it forms electrostatic diverging lens (field inhomogeneities cause that the particles from parallel beam gain perpendicular velocity, maximum divergence for edge points of the slit). Around the threshold energy $E = eV_\mathrm{b}$, the resolution is:

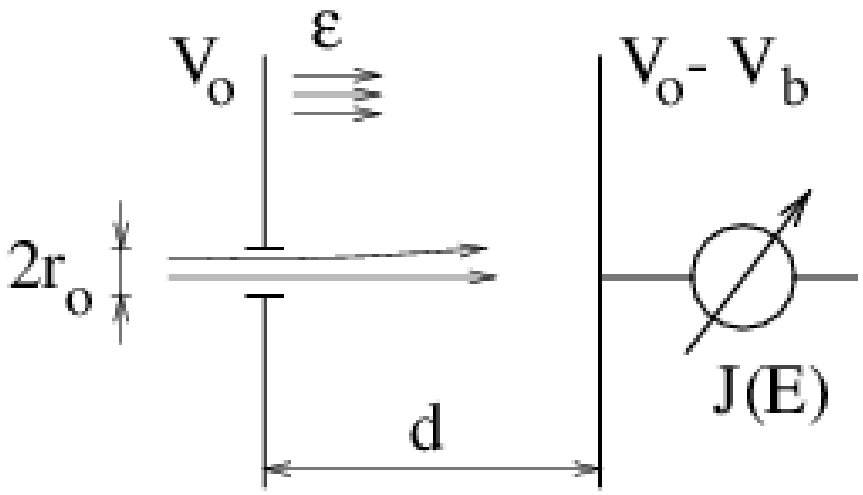

Figure 5.8: Scheme of planar analyser

$$R_{r_0} = \frac{16d^2}{r_0^2}. \tag{5.7}$$

The basic parameter is the diameter of the solid angle Ω, under which the beam enters the detector (effective area). Impute increases with the slit and Ω.

Spherical analysers

Compact electrode system often use a system of 3 or 4 grids (collectors). Total energy analysis is carried out in a radial trajectory of the particles. It can be used for LEED if the

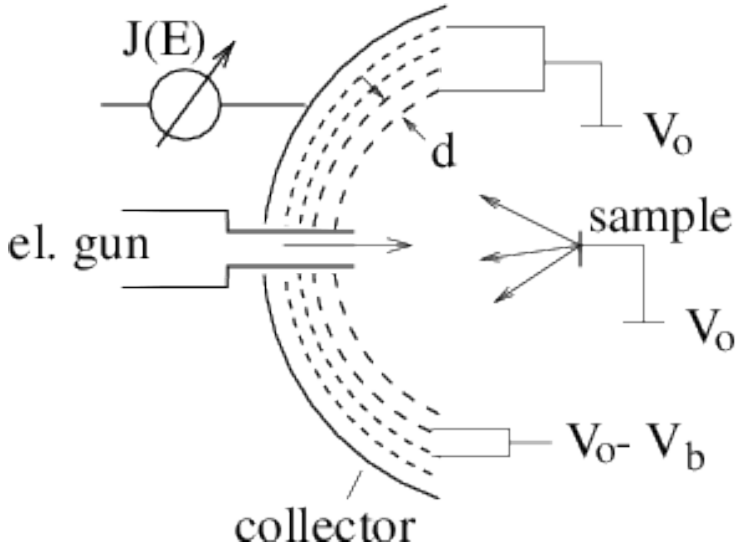

Figure 5.9: Scheme of spherical analyser

system in equipped with a fluorescent screen or a small movable detector. Retarding fields are generated between the 1st and 2nd (or 2nd and 3rd) grids. The resolution is given by the field inhomogeneity (mesh size, number of grids). Analyzer throughput is high because it can detect particles from a large solid angles (120° or 180°).

Dispersion analyzer (deflectors)

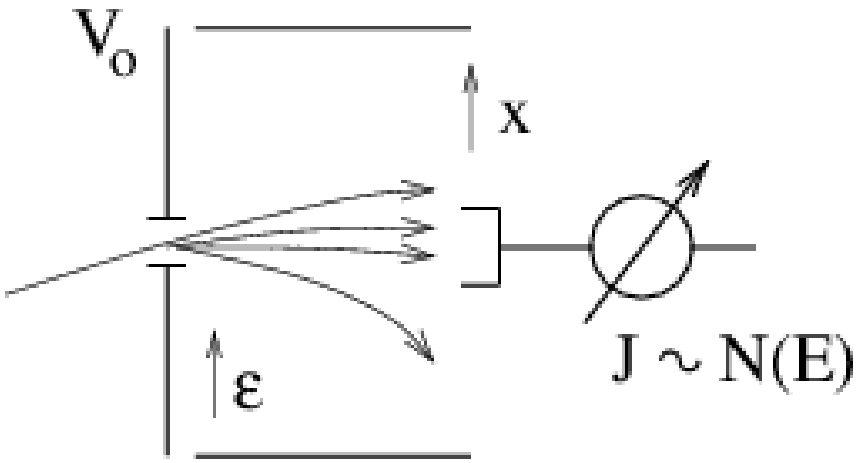

Figure 5.10: Scheme of dispersion analyzer

The parallel beam entering the analyzer is divided into different trajectories (Fig. 5.10) depending on the energy. The detector is either able to monitor signals at different positions (channel plate, screen) or it is tuned to detect particles with a certain energy E_0 (multiplier, Faraday cup). In the latter, a characteristic parameter is the main trajectory, i. e. the trajectory between the input and output slits. Properties of the analyzer are given by the *dispersion*

$$D(E) = E_0 \, \partial x / \partial E,$$

i. e. by the quantity expressing the difference in the position in the dependence on the energy. The dispersion with other parameters covering field focusation properties and some construction parts determines energy resolution of the analyzer.

Energy resolution can be estimated by detail analysis of particle trajectories in dependence on their input parameters: energy, coordinates of input slit, input angle. In most cases it is enough to use a rough estimate of the resolution as made below.

Let us irradiate the entrance slit s_1 by monoenergetic parallel beam that is imaged at the output slit with the magnification M. If the beam will be slightly divergent, each point of the entrance slit will be imaged by a line in each directions in which the focusation takes place. The length of this line is approximately

$$\Sigma \doteq a_1\alpha + a_2\alpha^2 + a_3\alpha^3 + \ldots + b_1\beta + b_2\beta^2 + b_3\beta^3 + \ldots . \tag{5.8}$$

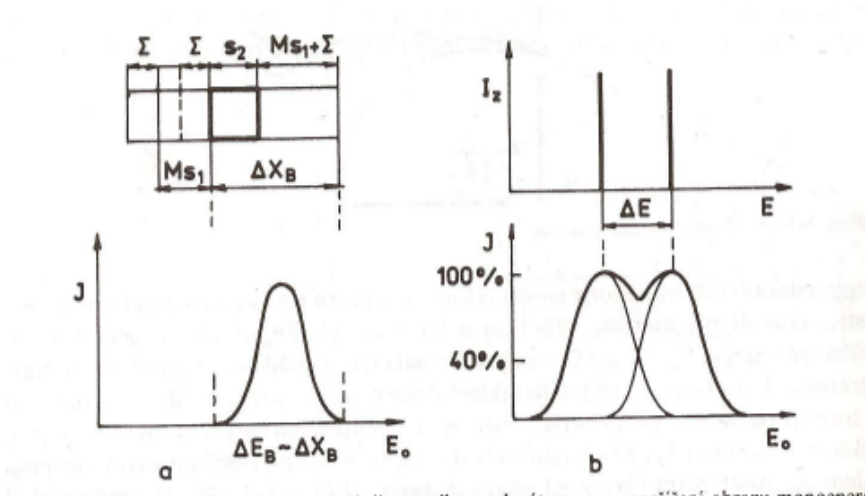

Figure 5.11: Understanding the energy resolution.

The angle 2α is divergence of the beam in the plane of the main trajectory, 2β in the plane perpendicular. The focusation order expresses how many coefficients $a_1, a_2, \ldots, a_n$ or $b_1, b_2, \ldots, b_n$ are equal to zero.

During anayzer tuning the image in output plane is moving. It is detected if some part of it falls into the output slit s_2. Its geometrical width is

$$\Delta x_B = M s_1 + s_2 + \Sigma \tag{5.9}$$

where s_1 and s_2 are the slit sizes for input and output, M is the magnification ($\sim$1) and Σ is the blur due to the input divergence. Δx_B is connected with energy width of the image in the vicinity of E_0 by

$$\Delta x_B = \frac{\partial x}{\partial E}\Delta E_B = \frac{D}{E_0}\Delta E_B. \tag{5.10}$$

It means that image of monoenergetic beam source is the peak with final width. If we have two such sources with close energies, they will be imaged with similar sensitivity as two close peaks (Fig. 5.11). They are expected as resolved if the minimum valey inbetween them is at 20 % of their maximum, i. e. they intersect at 40 % of their height. Their distance in energies ΔE will be approximately half of their energy base ΔE_B and we can write for the resolution R

$$R = \frac{E_0}{\Delta E} \doteq \frac{2E_0}{\Delta E_B} = \frac{2D}{\Delta x_B} = \frac{2D}{M s_1 + s_2 + \Sigma}\ . \tag{5.11}$$

From this expression is observed the decrease of R with the increase of slit size directly ($M s_1 + s_2$), and indirectly with Σ.

Dispersion analysers are divided into mirror and sector analyzers.

Mirror analyser

The beam enters through field lines at an different angle than $\pi/2$; the velocity component perpendicular to the field direction is maintained, $v_{\|}$ is gradually changed to the opposite direction

⇒ symmetrical axis trajectory ∥ to the field. The input and output slits are places in the positive potential electrode. The entrance angle is chosen with regard to the position of the source and the detector.

- planar - two parallel electrodes focusing only the deflection plane a. Two arrangements (a) $\phi_0 = \pi/4$, source and detector in the entrance and exit slits, (b) $\phi_0 = 30°$, source and detector tangent to field.
- cylindrical (CMA) - it is frequently used because allows the construction of high resolution systems. It consists of to concentric cylinders, with a positive potential between.

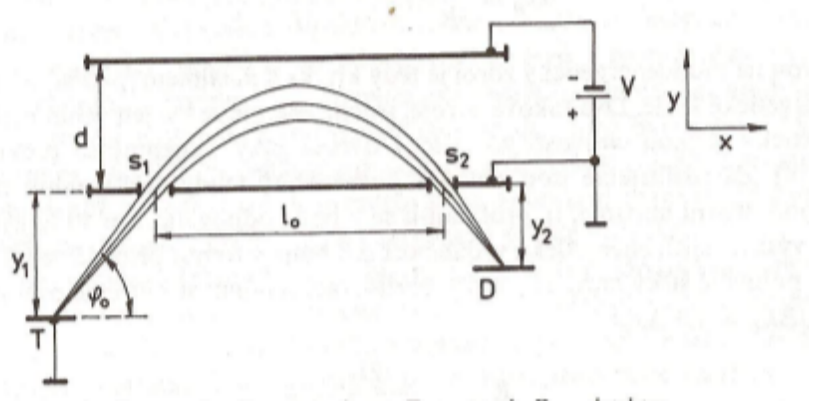

Figure 5.12: Scheme of planar mirror analyzer, T is sample, D is detector.

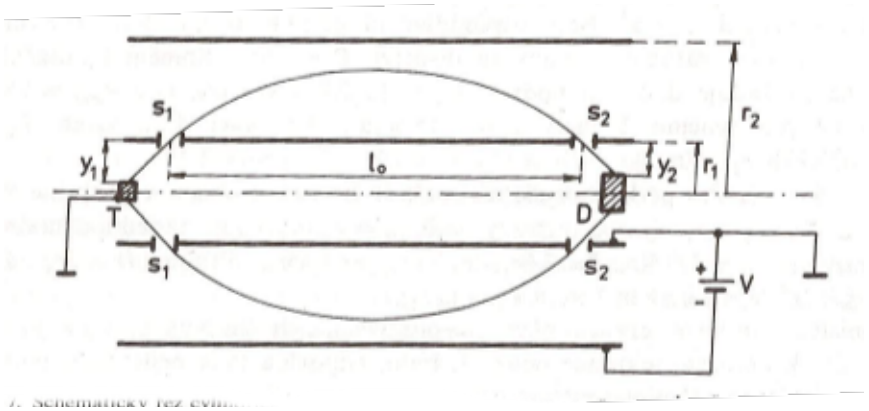

Figure 5.13: Scheme of CMA analyzer

Sectors analyzer

The beam enters ⊥ to the field. The main trajectory is a circle, where the centrifugal force associated with the kinetic energy compensates the centripetal force. The incident and reflected

angles is determined by the focus and position of the source and detector. It is mainly used in the differentiated angular spectroscopy:

- cylindrical - two cylindrical sector analyser and to pairs of planar electrodes (in front and lateral); in the frontal one are located the slits. Deflection potential $V_1 - V_2$ is inserted between the cylinders (inner potential is positive), both planar electrodes are isolated and maintained on the potential $V_0 = (V_1 + V_2)/2$. The analyser is focusing only in one direction. Sector angle is $\Phi = \pi/\sqrt{2} = 127,3^\circ$ therefore $\Rightarrow$ the name of 127° analyser.

- spherical (CHA - concentric hemispherical analyser) - two concentric spherical segments; input and output electrodes are radial slices are maintained at median surface potential V_0. The spherical deflector is capable of spatial focusing. Angle or the sector is usually $\Phi = 180^\circ$.

Conclusion
Analysing the energy of electrons has some other associated phenomena such as reflection and secondary emission. It is advantageous to use electron optics in order to increase the input angle, to obtain the image in a suitable place in the optimal regime area of the analyser, finely tune the input angle for slow electrons. The relative resolution of the analyser is constant $\Rightarrow$ absolute intensity will decrease with the decrease of energy.

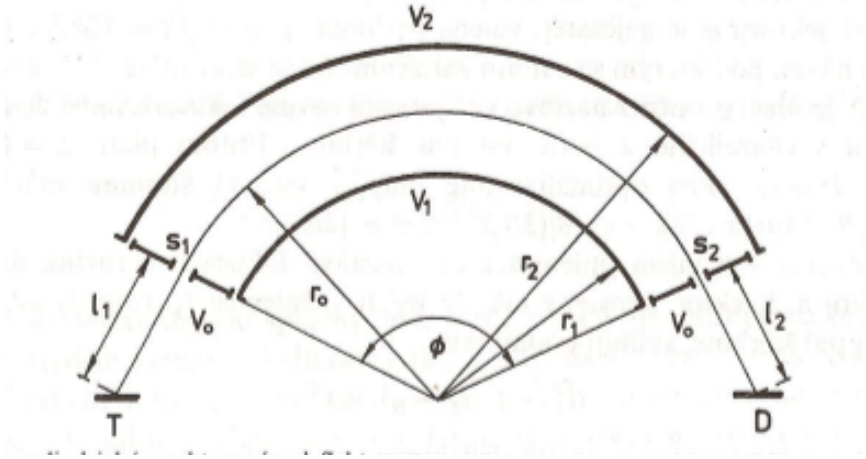

Figure 5.14: Scheme of cylindrical sector analyzer.

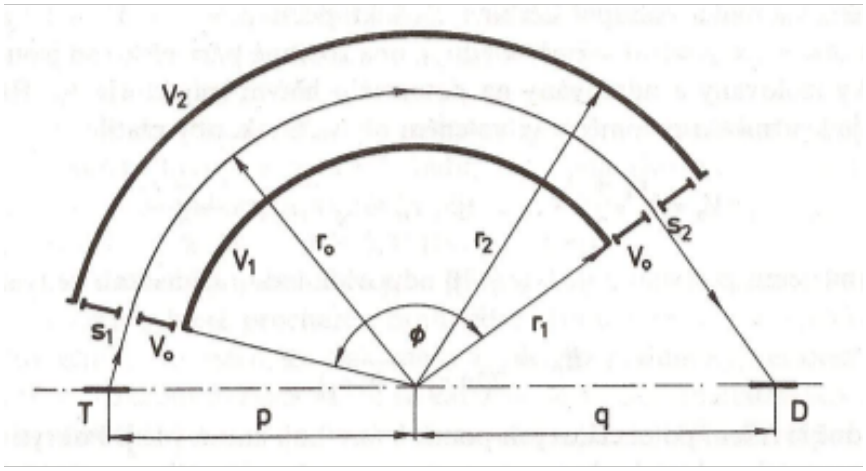

Figure 5.15: Scheme of spherical sector analyzer.

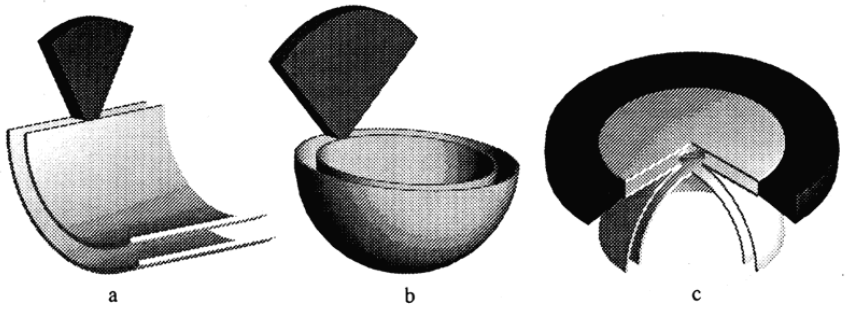

Fig. 1. Evolution of the electrostatic analyzer used in space plasma diagnostics: (a) cylindrical analyzer, (b) spherical analyzer, and (c) top-hat analyzer. The dark regions illustrate the field of view.

Figure 5.16: 3D view of sector analyzers.

5.4 Ultraviolet photoelectron spectroscopy

- If the photon energy is < 3 eV (VIS radiation), photoemission can occur only for substances with very low ϕ and the energy spectrum is narrow because e^- are emitted only from the highest occupied level $\Rightarrow$ information only about ϕ.

- If the photon energy is higher (UV radiation) electrons from the valence band can be emitted (UPS) $\Rightarrow$ distribution of densities of states in valence band can be obtained.

- In addition to energy distribution is possible to measure the angular distribution (ARUPS). In an isolated atom, the electrons occupy certain energy levels. In a solid, the levels involved in bonding 'the valence states', become blurred, and electrons can occupy a range of energies called bands. The energy of an electron in the solid depends on its momentum. Hence, by detecting photoelectrons emitted from a surface at different emission angles, the energy of the electrons as a function of the momentum vector may be determined. This process is known as "band mapping" and is a powerful probe of the electronic structure of crystalline materials.

- The mean free path in the case of UPS is only 0.5–2 nm $\Rightarrow$ surface characterization method.

Photoemission

The first paper of Burglund and Spicer (1964) worked out what is called the three-step model for photoemission, and the second applied it to new data on Cu and Ag. The three-step model uses this picture in considerable detail to predict the spectrum of photoelectrons from a given band structure. This spectrum sometimes resembles the density of occupied electronic states weighted by a function that varies smoothly with energy. This model assumes the photoemission process can be described by three sequential processes:

- photoexcitation of an electron (photoabsorbtion) - general theory based on Fermi's golden rule, which determines the transition probability between two electron states of the same Hamiltonian H^N, if the disturbance Δ is small.

$$w = \frac{2\pi}{\hbar} | < \psi_{\mathrm{f}}^N | \Delta | \psi_{\mathrm{i}}^N >^2 \ \ \delta(E_{\mathrm{f}}^N - E_{\mathrm{i}}^N - \hbar\omega) \tag{5.12}$$

- transport of that electron to the surface without inelastic scattering

- scape of the electron into the vacuum

The law of energy conservation must be applied ($E_{\mathrm{kin}} = E_{\mathrm{f}}^{\mathrm{u}} - e\Phi = E_{\mathrm{i}}^{\mathrm{u}} + \hbar\omega - e\Phi$) and the wavelength vector. Overall, the wave-vector is not maintained because the emitted electron escapes into vacuum, and the system achieve three-dimensional symmetry. The surface has only two-dimensional translation symmetry of the surface reciprocal lattice vector $\vec{G}_{\mathrm{S}}$:

$$\vec{k}_{\parallel}^{\mathrm{vn}} = \vec{k}_{\mathrm{f}\parallel}^{\mathrm{u}} + \vec{G}_{\mathrm{S}} \tag{5.13}$$

Inside the crystal the wave-vector is preserved:

$$\vec{k}_{\mathrm{f}}^{\mathrm{u}} = \vec{k}_{\mathrm{i}}^{\mathrm{u}} + \vec{G}_{\mathrm{B}}, \tag{5.14}$$

where $\vec{G}_{\mathrm{B}}$ is the reciprocal lattice volume vector. Dispersion relation for free e^-:

$$E_{\mathrm{kin}} = \frac{\hbar^2}{2m}(k_{\parallel}^2 + k_{\perp}^2). \tag{5.15}$$

If we don't know the dispersion relation within the crystal we are able to directly measure the band structure, but if we know the initial dispersion or the final states, we can limit the dispersion or the initial conditions. For surface conditions these restrictions do not apply ⇒ layered materials with two-dimensions periodicity exists: TaS_2, GeS or graphite, where the bulk band structure $E(k_{\parallel})$ will be explored.

$$k_{\parallel} = \sqrt{\frac{2m}{\hbar^2}\, E_{\mathrm{kin}}} \sin\theta, \tag{5.16}$$

where θ is the angle between the surface normal and the axis of the detector. The UPS method can be applied to absorb on substrate system like CO on Ni

Several modes exist for the evaluation of the emitted electrons:

- the number of emitted electrons is measured as the function of the final-state energy E_f (kinetic energy $E_k = E_f - E_{\mathrm{surf-barrier=E_f-e\Phi}}$ is measured) for a fixed photon energy and a fixed mutual position of the source and the surface elementary cell - energy distribution curve (EDC). EDC can be measured as integral or differential function of the emission angle. The latter is called angular resolved UPS (ARUPS).

- By scanning photon energy $h\nu$ and holding fixed the energy windows of the electron spectrometer, one measures the constant final-state spectra (CFS), $N(h\nu, E_f fixed)$. Unlike in EDC, the energy and wave vector are the same in every point of the spectra.

- By synchronously scanning $h\nu$ and E_f, so that $h\nu - E_f$, is held fixed, one measures the constant-initial-state spectra (CIS), $N(h\nu, h\nu - E_f fixed)$.

EDC
Přenesení počáteční hustoty stavů na hustotu prázdných konečných stavů vzdálených o $\hbar\omega$. Hlavní obtíž spočívá v oddělení příspěvků počátečních a koncových stavů. Tuto eliminaci je možné dostatečnou energií budící energie, aby e^- byly excitovány do oblasti, kde hustota tvoří prakticky kontinuum. Při energiích nad 100 eV to však vede ke ztrátě informací o impulzu e^-. Pro energie 30–100 eV jde o spektra zobrazující hustotu počátečních stavů a zachovávající možnost určení disperzních relací ⇒ synchrotronové záření. Musíme znát pásovou strukturu konečných stavů ⇒ aproximace model téměř volných e^-; kritické je umístění dna paraboly na energetické stupnici.

CFS
Elektrony jsou excitovány do jednoho zvoleného stavu ⇒ dává užitečné informace o výběrových pravidlech a symetrii stavů; pokud je okénko nastaveno tak, že leží mimo dovolené přechody

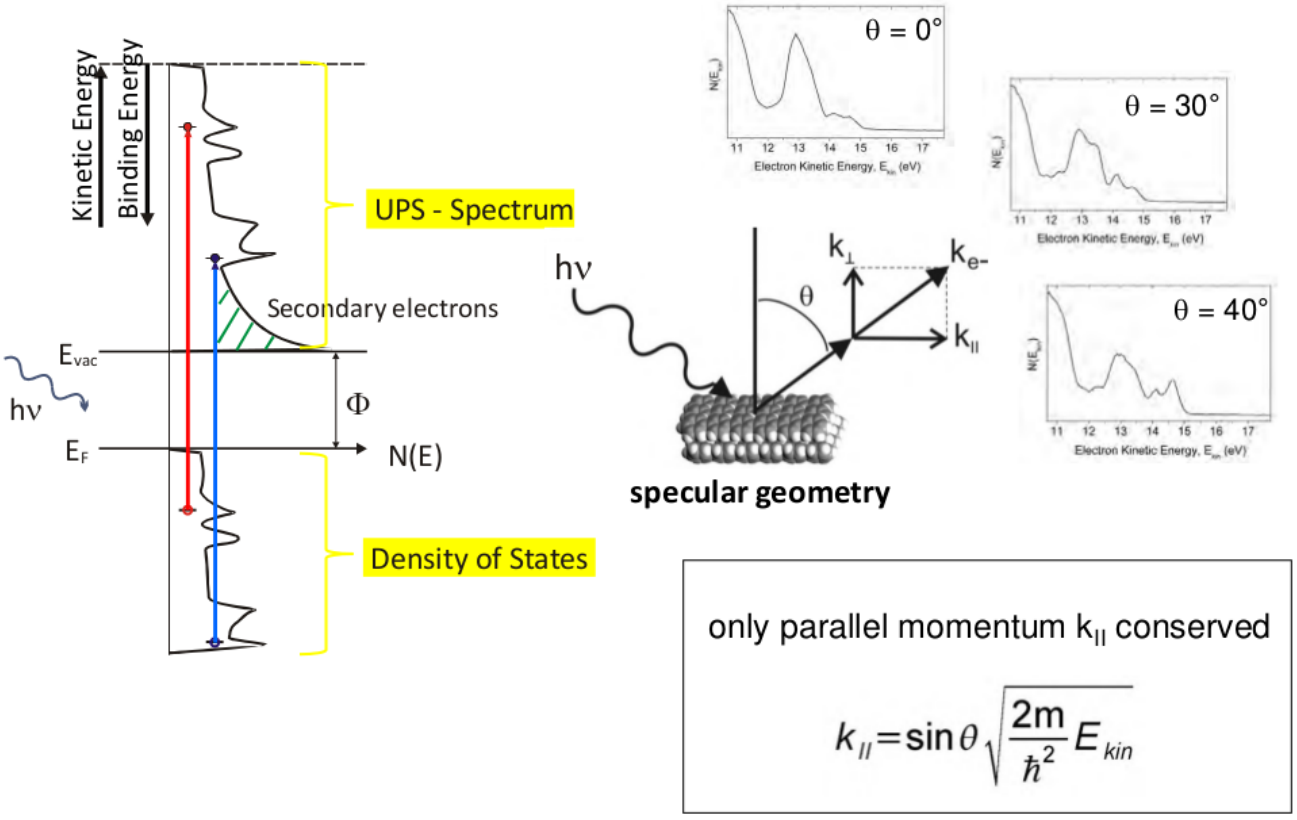

Figure 5.17: Angular resolved UPS.

v objemu, dominuje ve spektru příspěvek od povrchových stavů. Technika CFS je pro studium pásové struktury výhodnější než postup EDC, protože dovoluje snímat spektra s $\vec{k}_{\parallel}$ =konst i mimo normálu. Opět je nutné určit $\vec{k}_{\perp}$ vně PL a dát ji do souvislosti s odpovídající složkou vl. vektoru e^- v konečném stavu uvnitř PL $\Rightarrow$ postup obdobný jako u EDC.

CIS

Není tak rozšířena jako předchozí dvě techniky, protože byly vyvinuty jiné metody umožňující spektroskopii prázdných stavů v oblasti těsně nad dnem vodivostního pásu. U fotoemisních měření totiž nemohou e^- excitované do energetických pásů pod hladinou vakua přispívat k fotoproudu. Navíc se zvyšující se energií se zvětšuje energetické rozmazání pásů, a tím je velice obtížné získat informace o momentu e^- z úhlově rozlišených měření.

5.5 Spectroscopic nomenclature of electronic states

Molecules can possess several types of angular momentum. Electrons possess orbital and spin angular momenta, rotation of the molecule generates angular momentum, degenerate vibrations may give rise to vibrational angular momentum, and nuclei may also have spin angular momentum. Interactions (coupling) between these various types of angular momentum can have important implications for interpreting spectra, particularly high resolution spectra, and so it is important to be familiar with some basic results from the quantum theory of angular momentum.

The angular momentum is a vector quantity and a simple vector model provides a useful visual recipe for assessing how different angular momenta interact. There are more powerful and rigorous mathematical approaches to angular momentum coupling than that described here. These more comprehensive treatments deal explicitly with the angular momenta as mathematical operators, and the coupling behaviour then follows from the properties of these operators when added vectorially. The simple vector picture is use to emphasize the physical principles underlying the coupling of angular momenta, focussing on electronic angular momentum.

The magnitude of the orbital angular momentum for a single electron in an atom is given by the expression $\hbar\sqrt{l(l+l)}$ where l is the orbital angular momentum quantum number with allowed values 0, 1, 2, . . . Similarly, the magnitude of the spin angular momentum vector is given by $\hbar\sqrt{s(s+l)}$ where s is the spin quantum number which, for a single electron, can only take the value $1/2$. For an electron with both orbital and spin angular momenta, the total angular momentum vector j will be the sum of the two constituent vectors $j = l + s$. The magnitude of this vector is $\hbar\sqrt{j(j+l)}$, where j is the corresponding quantum number, and according to the quantum theory of angular momentum this can only take on the values $j = l+s, l+s-1, ..., |l-s|$. Series such as this are called Clebsch – Gordan series and arise when the total angular momentum results from a system composed of any two sources of quantized angular momentum. In the general case, if two angular momenta, say j_1 and j_2, can interact then the allowed values for the angular momentum quantum number for the resultant total angular momentum will be given by the Clebsch – Gordan series $j = j_1 + j_2, j_1 + j_2 - 1, ..., |j_1 - j_2|$

5.5.1 L-S (Russell-Saunders) coupling

In the Russell – Saunders limit the coupling between the orbital angular momenta is strong. The source of the coupling is the electrostatic interaction between two electrons. Electron spins can also couple together, although spin is a magnetic phenomenon and therefore the coupling is via magnetic fields,which tends to be a weaker effect than electric field coupling. In Russell – Saunders coupling the interaction between the orbital and spin angular momenta of a given electron is assumed to be small compared with the coupling between orbital angular momenta. In this limit the principal torque causes the orbital angular momenta to precess about a common direction, the axis of the total orbital angular momentum of all electrons. The spin angular momenta also couple together through the magnetic interaction of electron spins.

The vector model described above can be employed to see the effect of coupling on atoms.

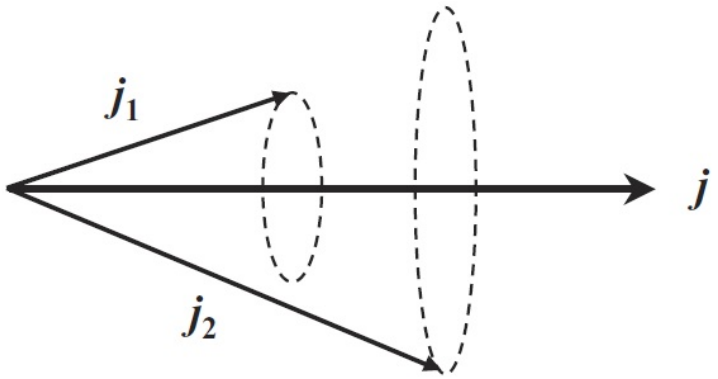

Figure 5.18: Forming the total angular momentum.

For illustration, consider an atom with two electrons outside its closed shell. The orbital angular momenta of these electrons are represented by l_1 and l_2, and the corresponding spin momenta by s_1 and s_2. The coupling of orbital angular momenta dominates and they form a resultant total orbital angular momentum $L = l_1 + l_2$. In the same way, the spin momenta also couple to form $S = s_1 + s_2$. When this coupling case is valid, the individual orbital angular momenta l_1 and l_2 precess rapidly around L, and s_1 and s_2 precess rapidly around S. L and S can themselves couple with each other, but this coupling, known as spin – orbit coupling, is assumed to be relatively weak. As a result, L and S precess slowly around the resultant total angular momentum $J = (L + S)$.

5.5.2 jj coupling

The Russell–Saunders scheme describes the electronic states of light atoms rather well but breaks down for heavier atoms, particularly for the lanthanides and actinides. This is due to increasing coupling between the orbital and spin angular momenta of individual electrons to the point where it is no longer negligible, as was assumed in the Russell – Saunders case. In the limit of very strong coupling between orbital and spin angular momenta, the appropriate coupling scheme is known as *jjcoupling*. A dominant spin – orbit torque will first couple the spin and orbital momenta of each electron to form resultants, $j_1 = l_1 + s_1$ and $j_2 = l_2 + s_2$. The vectors j_1 and j_2 interact more weakly, forming the total angular momentum $J = j_1 + j_2$. In jj coupling, $l_1(l_2)$ and $s_1(s_2)$ precess rapidly around $j_1(j_2)$, while jj_1 and j_2 precess slowly around their resultant J. As a result, only j_1, j_2, J and the projection of $J(M_J)$ are good quantum numbers, i.e. the quantum numbers L and S in the Russell – Saunders scheme have no significance in jj coupling. Of course it is also possible that the spin–orbit coupling is neither weak enough for Russell–Saunders to be applicable, nor strong enough for true jj coupling.

5.6 Auger electron spectroscopy

5.6.1 Auger effect

Auger electrons were named after Pierre Auger who, together with Lise Meitner, discovered Auger electron emission in 1920s. When a high-energy electron (or X-ray photon) strikes an inner shell electron of an atom, the energy of the incident particle can be high enough to knock out the inner shell electron. Thus, the atom becomes ionized and in an excited state. The atom will quickly return to its normal state after refilling the inner electron vacancy with an outer shell electron. In the meantime, the energy difference between the outer shell electron and the inner shell may cause emission of either an Auger electron from an electron shell or a characteristic X-ray photon. The kinetic energy of an Auger electron is approximately equal to the energy difference between binding energies in the electron shells involved in the Auger process. For example, the kinetic energy of an Auger electron is approximated by the following equation:

$$E_{KL1L2,3} = E_K - E_{L1} - E^*_{L2,3}, \tag{5.17}$$

where E_i is the binding energy and $E^*_{L2,3}$ is mark with asterisk because the energy levels $L^*_{2,3}$ differs slight from the energy levels of $L_{2,3}$.
The notation for kinetic energy of Auger electron describes its origin, but the nomenclature is rather complicated. For example, the kinetic energy of an Auger electron is from a following process: an incident electron knocks out a K shell electron, a L_1 shell electron refills the K shell vacancy, and a $L_{2,3}$ shell electron is ejected as the Auger electron. Auger electron spectroscopy (AES) identifies chemical elements by measuring the kinetic energies of Auger electrons. In an AES spectrum, an individual kinetic energy peak from an Auger electron is marked with an elemental symbol and subscripts indicating the electron shells or sub shells involved, for example, in aluminium oxide case, Al_{KLL}, O_{KLL}. . .

A typical AES spectrum is a plot of intensity versus kinetic energy; most commonly,it is a plot of the first derivative of intensity versus the kinetic energy. The primary electrons ejected from a solid surface by inelastic scattering comprise the background of an AES spectrum in the region of high kinetic energies while the secondary electrons comprise the background in the region of low kinetic energies. The number of Auger electrons ejected from a sample is much less than that of scattered primary electrons and secondary electrons. Thus, the direct-mode spectrum is not favoured except for quantitative analysis.

5.6.2 Fine Auger structure

A recent interest is concerned with the fine structures in the neighbourhood of Auger lines, denoted by EXAFS (extended X-ray absorption fine structure). It is a powerful nondestructive technique that provides structural information on metal or metal oxide phases highly dispersed on inorganic supports under reaction conditions. Bond lengths and coordination numbers of X-ray absorbing material can be determined. When single crystals are employed as supports, characterization of metal sites on them can be achieved separately in two different bonds parallel

and normal to the surface by polarized X-ray radiation.

In transmission mode, the EXAFS signal of surface species on solid substrates can not be detected because of the large adsorption by the substrate. To determine surface structures, it is possible to measure EXAFS spectra by detecting the reflected X-rays from sample, but usually the sensitivity is worse.

5.7 X-ray photoelectron spectroscopy

The X-ray photoelectron is an electron ejected from an electron shell of an atom when the atom absorbs an X-ray photon. An incident X-ray photon can have sufficient energy (a value of $h\nu$) to knock out an inner shell electron, for example from the atom's K shell. In such a case, the K-shell electron would be ejected from the surface as a photoelectron with kinetic energy E_K. Knowing the kinetic energy E_K, we can calculate the binding energy of the atom's photoelectron (E_B) based on the following relationship:

$$E_{\mathrm{B}} = h\nu - E_{\mathrm{K}} - \phi \tag{5.18}$$

The value of ϕ depends on both the sample material and the spectrometer. The binding energies (E_B) of atomic electrons have characteristic values, and these values are used to identify elements, similar to the way that characteristic X-ray energy is used in X-ray spectroscopy. X-ray photoelectron spectroscopy (XPS) identifies chemical elements from the binding energy spectra of X-ray photoelectrons.

Inner shell

- depending on how deep is, we obtain atomic number and the energy of X-rays
- doublet separations in photoelectron lines $\Leftarrow$ spin-orbital coupling jj. Splitting distance is directly proportional with $< 1/r^3 >$ for a given orbit, so it increases for higher Z or lower l (at constant n).

subshell	value of j	area ratio
s	$\frac{1}{2}$	–
p	$\frac{1}{2},\frac{3}{2}$	1:2
d	$\frac{3}{2},\frac{5}{2}$	2:3
f	$\frac{5}{2},\frac{7}{2}$	4:4

- Relative intensities are given by the photoemission cross section, analyser transmission and very little by the X-ray energy
- peak width (FWHM) is determined by

$$\Delta E = (\Delta E_{\mathrm{n}}^2 + \Delta E_{\mathrm{p}}^2 + \Delta E_{\mathrm{a}}^2)^{1/2}, \tag{5.19}$$

  where ΔE_{n} is the natural width of the inner surface, ΔE_{p} is the width of the X-rays ΔE_{a} is the analyser resolution (in all cases Gaussian distribution).

  – ΔE_{n} associated with the lifetime τ

$$\Gamma = \frac{h}{\tau}. \tag{5.20}$$

    where τ is related with the photoemission of X-rays, emission of Auger electrons or special type Auger electron (Coster-Kronig transition), which prefers l and is very fast. Width for light elements ($1s$, $2p$) increases with the atomic number.

– ΔE_a is constant for all peaks in "constant analyser energy" (CAE) mode, but changes in "constant retard ratio" (CRR), because $\Delta E/E$ ratio remains constant.

Valence shell
Electrons with low binding energy (0–20 eV). They are very close to each other ⇒ band structure. At high resolution spectrum scanning can show the band structure and a sharp decrease of intensity for E_F.

Auger series
Kinetic e^- energy from Coster-Kronig transition is very low; four basic series exists:

- KLL - from boron to magnesium(with Mg Kα) or aluminium (with Al Kα),
- LMM - from sulphur to germanium (with Mg Kα) or selenium (with Al Kα),
- $M_{4,5}N_{4,5}N_{4,5}$ - from molybdenum to neodymium (with Mg Kα),
- $M_{4,5}N_{6,7}N_{6,7}$ - only for high energy X-rays (e.g. Ag Lα, 2984 eV).

5.7.1 Energy scale calibration

For meaningful measurements it is important to ensure the instrument is calibrated. For example, to identify chemical constituents from the peak energy correctly, the energy scale needs to be calibrated. To provide quantitative information, use sensitivity factors and compare with other instruments, while the intensity scale needs to be linear and also corrected for the intensity response function. The intensity response function (IRF) includes the angular acceptance of the analyser to electrons, the transmission efficiency of electrons and the detection efficiency.

- for metals is possible to observe directly the Fermi level in the valence lines;
- the semiconductors are sufficiently conductive in order to offset the E_F. It is yet difficult to determine the exact location of line since the Fermi level depends on doping, surface states and defects;
- in the analysis of dielectrics the surface charge and energy shift occurs. The most commonly used method is called internal standard - a reference line from photoemission with a known binding energy from other measurements. It is based on the fact that often the sample is contaminated with hydrocarbons (C1s = 284,6–285,2 eV).

Cu and Au samples set with their angle of emission $\leq 56°$ are sputtered clean, and the measured energies of the peaks are compared with the energy values given in the table. As for AES, the peak energy for the calibration is evaluated from the top of the peak without background subtraction. For gold line $4f_{7/2}$ the energy is 83.95 eV. The lineshapes and energies of the $K_{\alpha 1}$ and $K_{\alpha 2}$ X-rays that characterize $h\nu$ appear to be the same in all unmonochromated instruments. However, the lineshapes and energies of the K_α X-rays, when monochromated vary significantly and depend on the set-up of the monochromator and its thermal stability. By

altering the monochromator settings, the measured energies of the peak may be moved over a kinetic energy range of 0.4 eV without too much loss of intensity.

Use of the standard with a modern, well-maintained spectrometer should result in calibration within tolerance limits of ±0.2 eV over four months or ±0.1 eV over one month before recalibration is required. For many purposes ±0.2 eV is satisfactory.

5.7.2 Primary structure information

Inner shell line
The binding energy is influenced by interactions with other electrons → chemical shift. The exact calculation of the binding energy is very difficult and limited to small molecules → approximate methods, such as electrostatic model - the model potentials(charge Potential model)

$$E_{\mathrm{B}} = E_{\mathrm{B}}^{0} + kq_i + \sum_{i \neq j} \frac{q_j}{4\pi\epsilon_0 r_{ij}}, \tag{5.21}$$

where E_{B}^{0} has significant calibration factor , k s a constant indicating an average repulsion between inner shell and valence e^{-}, q_i is the atom i charge and sum of potentials of neighbouring atoms j, also called Madelung potential, where r_{ij} are the internuclear distances.

Valence band peak
The valence electrons are directly involved in bond formation and molecular interactions, so the intensity and energy of the valence band peaks depend on their bonding environment. Thus, quantitative interpretation of the valence band spectrum for most materials requires a full molecular orbital calculation. For multi-component materials or those containing a large number of atoms per structural unit (e.g. polymers) this requires computer calculations.

Valence band analysis is worth pursuing because it can provide electronic structure information that cannot be obtained from typical core level analysis. Also, it is sometimes possible to extract useful structural information from valence band spectra.
In metals the information about the valence band and the Fermi energy give the opportunity to observe the transformation of the material from dielectric to metal (VO_2 non-conductor x metal at 65°, Na_xWO_3 non-conductor x metal when changing x).

Auger chemical shift
To identify the oxidation state of an element is often preferable to use the Auger parameter:

$$\alpha = E_{\mathrm{K}}(jkl) - E_{\mathrm{K}}(i) = E_{\mathrm{K}}(jkl) + E_{\mathrm{B}}(i) - h\nu, \tag{5.22}$$

where $E_{\mathrm{K}}(jkl)$ and $E_{\mathrm{K}}(i)$ is the kinetic Auger energy. α does not depends on the reference surface or the sample charge. The Auger parameter is modified

$$\alpha' = \alpha + h\nu = E_{\mathrm{K}}(jkl) + E_{\mathrm{B}}(i). \tag{5.23}$$

Auger line shapes
Auger lines can be readily distinguished from photoemission lines by changing X-ray sources (e.g.

using a Mg K_α source instead of an Al K_α source). If the Auger process causes the formation of at least one hole, then the distribution of Auger lines intensities strongly depends on the type of molecule.

5.7.3 Final state effects

X-ray satellites and ghost peaks
Satellites appear together with the less intensive X-ray characteristic peaks. The main peak $K\alpha_{1,2}$ corresponding to the $2p_{3/2,1/2} \rightarrow 1s$transition, satellites are $K\beta$, valence bands $\rightarrow 1s$ or multi ionized atoms.
Ghosts appear due to excitation of surface contaminants. Often, Al $K\alpha_{1,2}$ from the Mg $K\alpha$ (due to the aluminium window), followed by Cu $L\alpha$ and O $K\alpha$.

Multiplet splitting
A requirement for this splitting of the s photoemission peak into a doublet is that there be unpaired orbitals in the valence shells. Complex peak splitting can be observed in transition metal ions and rare earth ions when multiplet splitting occurs in p and d levels.

$$\Delta E = (2S^{\mathrm{v}} + 1)K_{\mathrm{sd}} \qquad \text{a} \qquad \frac{I(S^{\mathrm{v}} + 1/2)}{I(S^{\mathrm{v}} - 1/2)} = \frac{S^{\mathrm{v}} + 1}{S^{\mathrm{v}}}, \tag{5.24}$$

where S^{v} is the total spin of a unpaired valence electron and K_{sd} is the s-d exchange integral.

Shake-up satellites
It represents photoelectrons that have lost energy through promotion of valence electrons from an occupied energy level (e.g. a π level) to an unoccupied higher level (e.g. a pi^* level). Shake-up peaks (also called "loss peaks" because intensity is lost from the primary photoemission peak) are most apparent for systems with aromatic structures, unsaturated bonds or transition metal ions. In contrast to the continuum of reduced energies seen in the inelastic scattering tail, shake-up peaks have discrete energies ($\sim$ 6.6eV higher binding energy than the primary peak in C_{1s} spectra of aromatic-containing molecules) because the energy loss is equivalent to a specific quantized energy transition (i.e., the $\pi \rightarrow \pi^*$ transition).

Asymmetric metal lines
The metal lines may change with the degree of surface charging during data acquisition. With asymmetric metal lines as encountered with many transition metals, this effect may mimic the presence of metal ions, The line broadening is , most likely, due to varying degree of differential charging, since it is paralleled in the widths of the support elements.

Asymmetric non-metal lines
Appears only at high resolution. The asymmetry occurs due to fine vibrational structure of molecules. After ionization there is a change in interatomic distances and narrowing the potential curves of the molecule.

Shake-off satellites
If the departing photoelectron transfers sufficient energy into the valence electron to ionize it into the continuum, the photoemission loss peak is called a "shake-off" peak. The shake-off satellite peaks of the photoemission peak can have a wide range of possible energies (of course, always with a lower KE than the photoemission peak). This energetically broad feature is typically hidden within the background signal and is usually not detected or used analytically.

5.7.4 Angular effects

1. **Enhancement of system sensitivity and depth profile**
   Almost all electrons (95 %) come on a path equal with 3λ. If $e^-$are detected at angle θ different from normal, the thickness of the analysed layer is:

$$d = 3\lambda \sin\theta \tag{5.25}$$

   For the substrate (s) with homogeneous layer (v), the change of intensity in the ideal case is:

$$I^{\mathrm{s}}(d) = I_0^{\mathrm{s}}\, e^{-d/\lambda \sin\theta} \qquad \text{and} \qquad I^{\mathrm{v}}(d) = I_0^{\mathrm{v}}\, (1 - e^{-d/\lambda \sin\theta}). \tag{5.26}$$

   In practice, however, the geometry of the system also exhibits a angular response dependence function $\Rightarrow$ measured values for $I^{\mathrm{v}}/I^{\mathrm{s}}$

2. **Single-crystal studies**
   Measuring the absolute core electron intensity from a single-crystal surface, depending on the angle θ gives modulated intensity. Similar modulation is observed for fixed θ and rotation of surface plane. $\Rightarrow$ **X-ray photoelectron diffraction XPD**

5.8 Quantitative analysis in AES and XPS

Quantitative elemental analysis in electron spectroscopy is similar to that in X-ray spectroscopy. Analysis quantifies the concentrations of chemical elements on a sample surface from the peak intensities of the spectra. In theory, the quantitative relationship between the intensities of electron signals and atomic fractions of elements can be calculated. In practice, for quantification in both XPS and AES, most parameters for calculations are not available.

Sensitivity factor method: the Auger current is described by

$$I_{\alpha,\mathrm{XYZ}} = I_{\mathrm{p}} \gamma_{\alpha,\mathrm{XYZ}}\, T(E_{\alpha,\mathrm{XYZ}}) D(E_{\alpha,\mathrm{XYZ}}) \int_{E_{\alpha,\mathrm{X}}}^{E_{\mathrm{p}}} \sigma_{\alpha,\mathrm{X}}^{\mathrm{total}}(E) dE \int_0^{\infty} n_\alpha(z) e^{\left(-\frac{z}{\lambda^{\mathrm{M}}(E_\alpha)\cos\theta}\right)} dz \tag{5.27}$$

where I_{p} is the excitation current, $\gamma_{\alpha,\mathrm{XYZ}}$ is the Auger efficiency, $\sigma_{\alpha,\mathrm{X}}^{\mathrm{total}}(E)$ is the ionization cross section X the element α, E_{p} is the energy of the primary electron $n_\alpha(z)$ is the density of element α at depth z. The transmittance of the spectrometer is $T(E_{\alpha,\mathrm{XYZ}})$ and the sensitivity of the detector is $D(E_{\alpha,\mathrm{XYZ}})$.

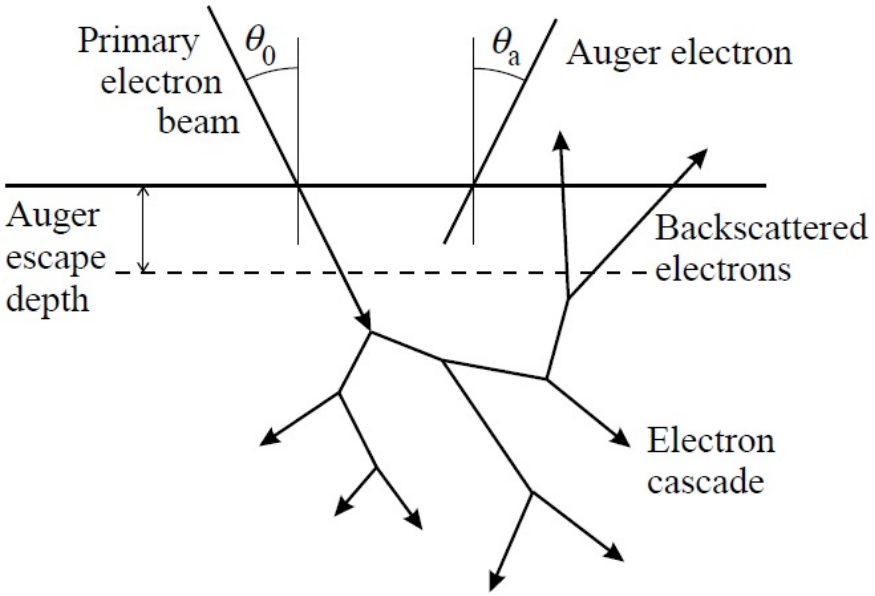

Figure 5.19: The physical processes occuring when an electron strikes a solid surface.

Ionization is caused not only by the electrons but also by the backscattered energy which has the distribution $n(E)$

$$\sigma_{\alpha,\mathrm{X}}^{\mathrm{total}} = \sigma_{\alpha,\mathrm{X}}(E_\mathrm{p}) + \int_{E_{\alpha,\mathrm{X}}}^{E_\mathrm{p}} \sigma_{\alpha,\mathrm{X}}(E) n(E) dE \tag{5.28}$$

This relation can be approximated as:

$$\sigma_{\alpha,\mathrm{X}}^{\mathrm{total}} = \sigma_{\alpha,\mathrm{X}}(E)[1 + r^{\mathrm{M}}(E_{\alpha,\mathrm{XYZ}}, \psi] \tag{5.29}$$

which can be simplified for homogeneous material

$$I_{\alpha,\mathrm{XYZ}} = I_\mathrm{p} \gamma_{\alpha,\mathrm{XYZ}}\ T(E_{\alpha,\mathrm{XYZ}}) D(E_{\alpha,\mathrm{XYZ}}) \sigma_{\alpha,\mathrm{X}}(E)[1 + r^{\mathrm{M}}(E_{\alpha,\mathrm{XYZ}}, \psi] n_\alpha \lambda^{\mathrm{M}}(E_\alpha) \cos\theta \tag{5.30}$$

The sensitivity factor $S_{\alpha,\mathrm{XYZ}}$ is defined as:

$$I_{\alpha,\mathrm{XYZ}} = I_\mathrm{p} n_\alpha \cos\theta\ S_{\alpha,\mathrm{XYZ}} \tag{5.31}$$

and the atomic concentration α in the M matrix

$$c_\alpha = \frac{n_\alpha}{\sum\limits_{\alpha'} n_{\alpha'}} = \frac{I_{\alpha,\mathrm{XYZ}}}{S_{\alpha,\mathrm{XYZ}}} \sum_{\alpha'} \frac{I_{\alpha',\mathrm{XYZ}}}{S_{\alpha',\mathrm{XYZ}}} \tag{5.32}$$

The sensitivity factor must be determined either theoretically or directly experimentally. Common practice is to use the sensitivity factors from published handbooks with certain corrections according to the instrument characteristics, because it is not feasible to compile a set of in-house sensitivity factors.

Standard method: For simplicity, a binary alloy $\alpha\beta$ is selected. No contamination on the surface or segregation phenomena exists:

$$\frac{I_\alpha}{I_\alpha^{\rm s}}\frac{I_\beta^{\rm s}}{I_\beta} = \frac{n_\alpha}{n_\beta}\ \left(\frac{n_\alpha^{\rm s}}{n_\beta^{\rm s}}\ \frac{\lambda_\alpha\lambda_\beta^{\rm s}}{\lambda_\beta\lambda_\alpha^{\rm s}}\ \frac{(1+r_\alpha)(1+r_\beta^{\rm s})}{(1+r_\beta)(1+r_\alpha^{\rm s})}\right) = \frac{n_\alpha}{n_\beta}\ K \tag{5.33}$$

and the elemental concentration α is

$$c_\alpha = \left(1+\frac{I_\beta I_\alpha^{\rm s}}{I_\alpha I_\beta^{\rm s}}\frac{1}{K}\right)^{-1}. \tag{5.34}$$

The matrix correction factor K describes the influence of the $\alpha\beta$ alloy. When $K=1$, we assume that the influence on matrix is negligible.

Quantitative analysis - old text for XPS

The intensity of the photoemission line i

$$I_{\rm A}^i \sim Q\mathcal{A}\ c_{\rm A}\sigma_{\rm A}^i\lambda^i T^i L_{\rm A}^i f(\phi,\theta), \tag{5.35}$$

where Q is the photon flux [$\mathrm{cm^{-1}s^{-1}}$], $\mathcal{A}$ effective are of the sample, $c_{\rm A}$ concentration of A, $\sigma_{\rm A}^i$ is the partial ionization cross section, λ^i mean free path, T^i the transmission, $L_{\rm A}^i$ angular asymmetry coefficient and $f(\phi,\theta)$ function, depending on the geometry of the experiment. The above equation does not detect the absolute concentration of elements. The intensities of the lines for individual measured elements under the same conditions can determine the relative atomic composition. When a solid is homogeneous within the analysed depth for all elements of interest (A and B for example), the uncertainties can be partially cancelled by considering relative atomic values. We obtain:

$$\frac{I_{\rm A}^i}{I_{\rm B}^j} = \frac{c_{\rm A}\sigma_{\rm A}^i\lambda^i T^i L_{\rm A}^i}{c_{\rm B}\sigma_{\rm B}^j\lambda^j T^j L_{\rm B}^j} = \frac{c_{\rm A}\sigma_{\rm A}^i L_{\rm A}^i}{c_{\rm B}\sigma_{\rm B}^j L_{\rm B}^j}R. \tag{5.36}$$

If the kinetic energy differs by more than ~ 400 eV, correction of T and λ should be performed. the correction used for transmission:

$$T \sim 1/E_{\rm k} \qquad \text{for constant energy (CAE)} \tag{5.37}$$

and

$$T \sim E_{\rm k} \qquad \text{for constant resolution (CRR).} \tag{5.38}$$

To calculate the mean free path, the typically used equation is

$$\lambda = aE_{\rm k}^{-2} + bE_{\rm k}^{1/2}. \tag{5.39}$$

One of the major problem in quantitative analysis is the integral of photoemission intensity lines. When using the theoretical values σ we have determine the overall intensity of lines including the contributions of all satellites and inelastic electron scattering. For practical purposes we can use the equation:

$$\frac{I_{\rm A}^i}{I_{\rm B}^j} = \frac{c_{\rm A}S_{\rm A}^i}{c_{\rm B}S_{\rm B}^j}. \tag{5.40}$$

The intensity of the photoemission line i

$$I^i_{\mathrm{A}} \sim Q\mathcal{A}\, c_{\mathrm{A}}\sigma^i_{\mathrm{A}}\lambda^i T^i L^i_{\mathrm{A}} f(\phi,\theta), \tag{5.41}$$

where Q is the photon flux [$\mathrm{cm}^{-1}\mathrm{s}^{-1}$], $\mathcal{A}$ effective are of the sample, c_{A} concentration of A, σ^i_{A} is the partial ionization cross section, λ^i mean free path, T^i the transmission, L^i_{A} angular asymmetry coefficient and $f(\phi,\theta)$ function, depending on the geometry of the experiment. The above equation does not detect the absolute concentration of elements. The intensities of the lines for individual measured elements under the same conditions can determine the relative atomic composition. When a solid is homogeneous within the analysed depth for all elements of interest (A and B for example), the uncertainties can be partially cancelled by considering relative atomic values. We obtain:

$$\frac{I^i_{\mathrm{A}}}{I^j_{\mathrm{B}}} = \frac{c_{\mathrm{A}}\sigma^i_{\mathrm{A}}\lambda^i T^i L^i_{\mathrm{A}}}{c_{\mathrm{B}}\sigma^j_{\mathrm{B}}\lambda^j T^j L^j_{\mathrm{B}}} = \frac{c_{\mathrm{A}}\sigma^i_{\mathrm{A}} L^i_{\mathrm{A}}}{c_{\mathrm{B}}\sigma^j_{\mathrm{B}} L^j_{\mathrm{B}}} R. \tag{5.42}$$

If the kinetic energy differs by more than ~ 400 eV, correction of T and λ should be performed. the correction used for transmission:

$$T \sim 1/E_{\mathrm{k}} \qquad \text{for constant energy (CAE)} \tag{5.43}$$

and

$$T \sim E_{\mathrm{k}} \qquad \text{for constant resolution (CRR).} \tag{5.44}$$

To calculate the mean free path, the typically used equation is

$$\lambda = aE_{\mathrm{k}}^{-2} + bE_{\mathrm{k}}^{1/2}. \tag{5.45}$$

One of the major problem in quantitative analysis is the integral of photoemission intensity lines. When using the theoretical values σ we have determine the overall intensity of lines including the contributions of all satellites and inelastic electron scattering. For practical purposes we can use the equation:

$$\frac{I^i_{\mathrm{A}}}{I^j_{\mathrm{B}}} = \frac{c_{\mathrm{A}} S^i_{\mathrm{A}}}{c_{\mathrm{B}} S^j_{\mathrm{B}}}. \tag{5.46}$$

5.9 Numerical data analysis

Simple operation with data:
(a) integration and determination of area, (b) noise removal, (c) satellites removal, (d) background subtraction, (e) addition and subtraction of spectra, (f) search for lines maxima, (g) conversion to the binding energy after calibration.

background subtraction

- linear background: straight line between the first and last point of the spectrum
- integral background: the integral is calculated over the hole line area and a calibrated curve thus obtained is subtracted from the peak area

- background based on the elastic and inelastic processes

Signal to noise ratio

The noise is characterised in three different ways: peak-to-peak (p.t.p.), root-mean-square (r.m.s.), standard deviation. If the spectrometer is limited to statistical noise, the signal to noise ratio (S/N) can be defined like:

$$S/N = \sqrt{\frac{S+B}{F}}, \tag{5.47}$$

where S is the height of the line above background B, is the background B and F is the intensity factor

$$F = \frac{(S/B+1)(S/B+2)}{(S/B)^2}. \tag{5.48}$$

If we desire S/N constant

$$t_2/t_1 = F_2/F_1. \tag{5.49}$$

Smoothing

- fitting the data with a suitable smooth function (polynomial, fractional polynomial, exponential, Fourier and splines)
- convolution data using a suitable algorithm, which leads to a smoothing

$$y_r^{\mathrm{sm}} = \sum_{r=-m}^{m} \frac{C_r y_r}{\mathrm{NORM}}, \tag{5.50}$$

  where C_r is the convolution number and NORM is the normalizing factor. Savitsky-Golay convolution is recursive. the convolution function represented by lest squares fitting of an polynomial(cubic-quadratic) to m points on either side of each data point.

- frequency filter for Fourier transformation (mathematical equivalent of convolution algorithm).

Analysis of overlapping spectral lined

- spectra derivation (background removal, separation of overlapping lines), negative lines in the second derivative correspond to approximately the position of overlapping lines ⇒ noise problems ⇒ smoothing with derivation
- deconvolution, mostly for the shape of the line

$$y_j^{\mathrm{m}} = \sum_{i=1}^{N} y_i^{\mathrm{t}} g_{j-1} \; + \; n_j, \tag{5.51}$$

  where n_j is the noise. The instrument function g can be determined by line measurement of Ag 4 eV from the Fermi level with a monochromatic X-ray source.

- fitting with Gaussian or Lorentz function. It can either be used the Voigt convolution or a mix Gauss-Lorentz function

$$f(E) = \frac{A}{[1 + M(E - E_0)^2/\beta^2] \exp([1 - M][\ln 2(E - E_0)^2]/\beta^2)}, \tag{5.52}$$

  wheree M is mixing ration (1 for pure Lorentz shape) and β is a parameter, which is nearly 0.5 FWHM.

5.10 Electron energy loss spectroscopy

Metoda EELS je založena na **nepružném rozptylu primárních e$^-$** pevnou látkou, při níž dochází k vybuzení e$^-$ nebo skupiny e$^-$ (vybuzení plazmonů) pevné látky do vyššího stavu.
Hodnoty **energie primárních e$^-$** jsou několik **desítek eV** $\Rightarrow$ povrchová metoda.

Elektrony přecházejí do vyšších hladin téhož pásu (vnitropásové přechody), do jiného pásu (mezipásové přechody) nebo do povrchových stavů. $\Rightarrow$ Měřením ztrát získáme představu o elektronové struktuře PL - neobsazených stavech. Musíme mít ovšem nezávislou informaci o rozdělení a polohách zaplněných stavů, např. z fotoelektronové spektroskopie.
Hodnoty **energetických ztrát jsou 1–20 eV**.
The laws of energy and impulse conservation forms

$$E'(\vec{k}') = E_0(\vec{k}) - \hbar\omega, \tag{5.53}$$

$$\vec{k}'_{\parallel} = \vec{k}_{\parallel} - \vec{q}_{\parallel} \pm \vec{g}_{\parallel}, \tag{5.54}$$

where $E_0(\vec{k})$ is the incident e$^-$energy with momentum $\hbar\vec{k}$, $E'(\vec{k}')$ is the backscattered e$^-$energy with momentum $\hbar\vec{k}'$, $\hbar\omega$ is e$^-$energy loss in the transmission, $\vec{q}$ is the transferred momentum $\vec{g}$ is the lattice reciprocal vector.

EELS modifications: AREELS - Angle Resolved EELS, HREELS - High Resolution EELS (rozptyl na fononech povrchových vibrací, ztráty jsou ≈ 0.1 eV.), pro vysokou energii primárních e$^-$ (několik desítek keV) je možno měřit i v transmisním módu.

Experiment: HV nebo UHV (pro výzkum povrchů), zdroj primárních e$^-$(v případě HREELS monochromatizovaných) a kolektor rozptýlených e$^-$ (čtyřmřížkový analyzátor s brzdným polem užívaný pro LEED nebo válcový zrcadlový analyzátor CMA používaný pro Augerovskou spektroskopii). AREELS lze provádět v optice LEED za pomoci bodového fotometru nebo úpravou jednoduššího systému s rovinnými mřížkami a stínítkem a elektronovým násobičem. Měření rozptylu rychlých e$^-$ lze s výhodou provádět v transmisních elektronových mikroskopech.

Jsou možné tři nezávislé způsoby měření spekter:

1. Měření při konst. úhlech θ, θ' a konst. hodnotě energetické ztráty $\hbar\omega$ v závislosti na primární energii e$^-$, tzv. energetické profily ztrát
2. Měření vybrané ztráty $\hbar\omega$ při konst. $\vec{k}$ v závislosti na úhlu rozptylu θ'.
3. Měření při konst. $\vec{k}'$ rozptýlených e$^-$ v daném směru v závislosti na velikosti energetické ztráty, tzn. proměřování spektra ztrát energie při dané energii a směru dopadajících e$^-$ ve směru daném detektorem.

Základním problémem po naměření spekter je přiřazení naměřených ztrát energie rozptylovým mechanismů. Nejprve se sanžíme určit plazmové ztráty a pak mezi zbývajícími maximy rozlišit objemové (ozn. E) a povrchové procesy (ozn. S). Často jsou zastoupena i maxima odpovídající ionizaci hlubších hladin (např. “d”).

EELS poskytuje informace o struktuře PL a doplňuje tak informace získané jinými povrchově citlivými metodami, např. XPS.

5.11 Threshold techniques

An alternative form of core level spectroscopy is based on the detection of the onset on ionization as the exciting beam energy passes through such a threshold (equal to the binding energy of the core level relative to the Fermi level of the solid). A technique of this kind involves sweeping the exciting energy beam and detecting the onset of emission of photons or Auger electrons associated with the refilling of the core hole thus created. These different modes of detection form a group under the general heading of APS (Appearance Potential Spectroscopy). In principle, either incident electrons or photons could be used but the photon calls for a tunable light source in the 50–2000 eV range, only possible using synchrotron radiation.
All three modes of the incident electron technique have been used, however, the thresholds either being detected by fall in the elastically scattered electron flux (Disappearance Potential Spectroscopy - DAPS), by the onset of photons emission (Soft X-ray Appearance Potential Spectroscopy - SXAPS) or by the onset of the new Auger electron emission channel (Auger Electron Appearance Potential Spectroscopy - AEAPS). Note that in all of these techniques the surface sensitivity is guaranteed by inelastic scattering of the incident electron beam.
Primary energy E_p is determined by:

$$E_\mathrm{p} = eV_\mathrm{p} + \phi + kT. \tag{5.55}$$

By applying the conservation of energy

$$E_\mathrm{p} - E_1 = E_\mathrm{B} + E_2, \tag{5.56}$$

where E_1 is the primary electron energy level, E_B is the binding energy of the electron on the surface E_2. At the threshold energy can be captures just above the Fermi level i.e.$E_1 = E_2 = 0$ and E_p=E_B. If instead of thermionic cathode we have tunnel cathode, the $eV_\mathrm{p} = E_\mathrm{B}$. The probability of excitation of the inner layers is:

$$W(E_\mathrm{p}) \approx \int_0^{E_\mathrm{p}} \psi(E' - E_\mathrm{B}) \int_0^{E_\mathrm{p}+E'} \tag{5.57}$$